Korean J. Chem. Eng., 40(3), 532-538 (2023)
DOI: 10.1007/s11814-023-1386-2

pISSN: 0256-1115
eISSN: 1975-7220

Effect of particle morphology on the fast-charging properties of high-nickel cathode materials

Yang Soo Kim‡, Jongmin Kim‡, Chang-Su Kim, Yong Min Kwon, Seong In Kim, and Ji-Yong Eom†

Chemical Materials R&D Department, Korea Automotive Technology Institute Cheonan, Chungnam 31214, Korea
(*Received 29 August 2022 • Revised 13 December 2022 • Accepted 23 December 2022*)

Abstract−In order to investigate the effect of the particle morphology on the fast-charging characteristics of high-nickel layered-cathode materials, single-crystalline and secondary-particle type cathode with different primary/secondary particle sizes were synthesized via careful microstructure design. The effect of crystalline and particle size on the fast-charging performance was identified by comparing the charging characteristics at various current rates. Also, the effect of rapid charging on the cycle-life performance of the high-nickel cathode materials was confirmed through repeated fast-charging experiments. The size of the primary particle (crystalline size) has a greater effect on the rapid-charging performance than the entire particle size. In addition, to suppress the performance degradation of high-nickel cathode during fast charging, it is important to suppress the increase in the surface area through micro-crack suppression, and it is also necessary to precisely control the size of the primary particle for efficient lithium diffusion during fast charging.

Keywords: Fast Charging, High Nickel, Layered-Cathode Material, Single Crystalline, Secondary Particle

INTRODUCTION

Currently, lithium-ion batteries (LIB) are used in a wide variety of devices, and the LIB market is expected to grow more than five times over the next ten years. In particular, the rapid spread of mid- to large-sized batteries for electric vehicles (such as EV, PHEV, HEV) and energy storage systems (ESS) will drive market growth. In addition, with the abrupt increase in the mobile device and electric vehicle (EV) market, the fast-charging performance of batteries has become an important issue for improving user convenience. Recently, high nickel based layered oxide received a great deal of attention as a high capacity cathode material due to their excellent energy density and high-rate performance [1]. However, as nickel content increases, the lattice change of layered structure caused by lithium intercalation becomes larger, which causes microcracks at the grain boundary between primary particles constituting the polycrystals, resulting in degradation of cycle-life performance, increased gas generation, and safety hazard [2]. Also, fast charging further accelerates crack generation and performance degradation [3]. As an alternative to overcome these intrinsic problems of the polycrystal morphology of high-nickel cathode, single-crystal type cathode material is attracting attention because of excellent cycle-life performance and better safety as well as reduced gas generation during repeated cycling [4]. However, in the case of a single crystal, since there is no grain boundary, lithium can diffuse only through the lattice, the capacity and high-rate characteristics would be limited as the size of the crystal increases [3]. Fast-charging characteristics of cathode materials are greatly affected by lithium diffusion, crack generation, and primary/secondary particle size [5,6]. Chen's group studied the effect of crystal planes on lithium diffusion by comparing single and secondary particles with different morphologies. However, since the crystalline size between single and secondary particle was similar, the effect of primary- and entire particle size on the rate performance could not be separated [3]. Janek's group investigated the effect of charging on the structural degradation of single and secondary particles [7]. Nevertheless, the effect of the particle morphology on the fast charging characteristics is still unclear, and there is still no literature confirming the rapid charging characteristics by controlling the morphology of primary/secondary particles in the high-nickel cathode materials with similar composition. In this study, large secondary particle with small crystalline size and two single crystal-type particles with different crystalline size were synthesized via precise process control. And the effect of particle morphology on the lithium diffusion properties and structure deterioration was analyzed through repeated fast-charging experiments.

EXPERIMENTAL

1. Material Synthesis

To obtain active materials of high-nickel single crystal and secondary particle type cathode, metal-hydroxide precursor powder ($Ni_{0.92}Co_{0.04}Mn_{0.04}(OH)_2$) and lithium hydroxide ($LiOH{\cdot}H_2O$) were thoroughly mixed by a laboratory blender. Single crystal with Li/transition metal (TM) ratio of 1.05 was used, and secondary particles with Li/TM ratio of 1.02 were prepared. To obtain single crystal-type particles with different crystalline sizes, mixed powders were calcined at 900 °C (S1) and 940 °C (S2) for 10 h in oxygen atmosphere in a tube furnace, respectively. As-synthesized single crystal-type aggregates were pulverized through a high-energy ball mill

†To whom correspondence should be addressed.
E-mail: jyeom@katech.re.kr
‡These authors contributed equally to this work.

(8000M Mixer/Mill, SPEX SamplePrep). Also, to restore the damaged surface properties during ball milling, pulverized powders were coated with Co through secondary thermal treatment at 750 °C. In the case of secondary particles (L1), mixed powders were calcined at relatively low temperatures of 600 °C for 2 h and 760 °C for 10 h to suppress grain growth.

2. Characterization

To fabricate the cathode electrodes, the synthesized active materials were mixed with a conducting agent (Super P), binder (Solef 6020 polyvinylidene fluoride (PVDF), Solvay) in a weight ratio of 96 : 2 : 2 in N-methyl-2-pyrrolidone (NMP) using a Thinky mixer (ARE310, Thinky) to form a slurry. The slurry was single side coated on Al foil as a current collector with a mass loading of ~10 mg/cm^2. After the slurry was dried, the electrodes were roll-pressed and punched (diameter 14 mm). Then, the punched electrodes were dried in a vacuum oven at 100 °C overnight. The 2032 coin-type half cells were assembled in an argon-filled glovebox, using prepared electrode as cathodes, Li metal foil (700 μm, Honjo) as anodes, 1.0 M LiPF6 in EC/DEC 3 : 7 (v/v) with FEC 5% additive as an electrolyte, and porous polyethylene as a separator. The rate capability and cycle performance were tested at voltage between 3 V and 4.3 V (versus Li/Li$^+$) at room temperature (25 °C) in the range between 0.1 C and 10 C using a battery cycler system (WBCS3000, WonATech). The electrochemical impedance was measured using an impedance analyzer (ZiVE MP2, WonATech).

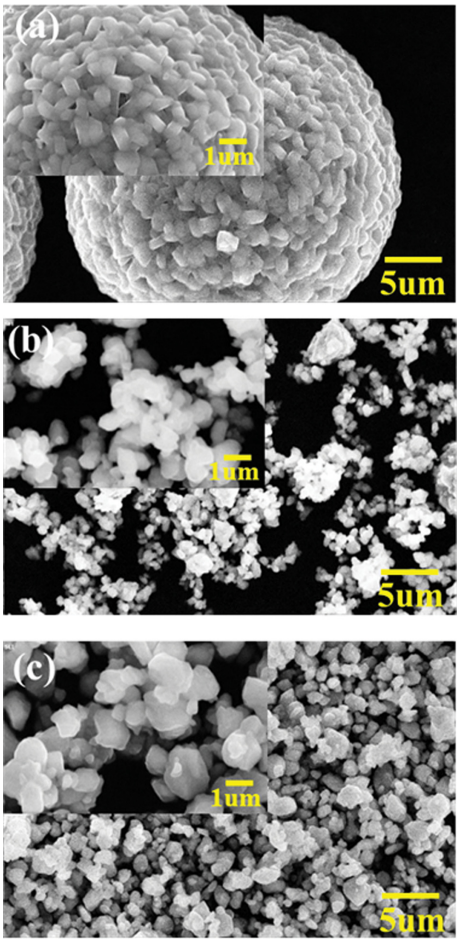

Fig. 1. SEM images of cathode particle with different morphology, (a) secondary particle (L1), (b) single particle (<1 μm) (S1), (c) single particle (>1 μm) (S2).

RESULTS AND DISCUSSION

1. Morphology

The morphology of secondary and single-crystalline type particles was identified by scanning electron microscopy (SEM), as shown in Fig. 1. In the secondary particle type cathode material (L1), small crystals of <500 nm form 15 μm-sized aggregates (Fig. 1(a)). Figs. 1(b) and (c) show the SEM images of single-particle type cathode materials composed of a single or several crystals. The single-crystalline type particle (S1) synthesized at a temperature of 900 °C has a grain size of 500-1 μm (Fig. 1(b)) and the other single-crystalline type particle (S2) has larger grain size of 1 μm to 2 μm (Fig. 1(c)), as grain growth was promoted at a higher 940 °C [4].

2. Initial Capacity

An initial charge/discharge cycling test was performed to confirm the capacity of the secondary and single-crystalline type cathode materials (Fig. 2). The initial discharge capacity (0.1 C, 20 mA) of all three types of particles exhibits >210 mAh/g, which shows excellent performance of high-nickel cathode materials. The charge capacity of three types of particle is similar; however, there is slight difference in the discharge capacity. S1 with the smallest particle size shows the best initial capacity value (220.7 mAh/g); the discharge capacity of S2 is 217.5 mAh/g; L1 shows a relatively low initial capacity of 212.8 mAh/g. The difference in the discharge capacity is considered to be due to the specific surface area of each particle. In the case of the large secondary particle (L1), despite the small size of the primary particle (500 nm), the size of the spherical aggregates (15 μm) is relatively much larger than that of the single crystal. For this reason, the specific surface area is smaller than single-type particle, and consequent lithium diffusion through the particle surface will be limited; as a result, a relatively low initial capacity value of L1 is shown. Among the same single-crystal active mate-

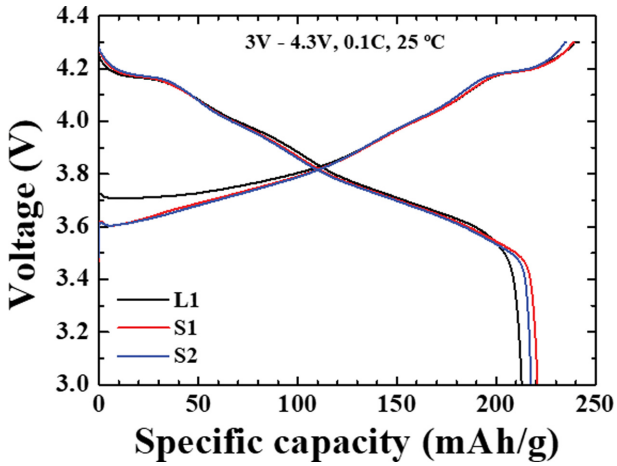

Fig. 2. Initial charge-discharge voltage profiles of cathode particle with secondary particle (L1), single particle (<1 μm) (S1), single particle (>1 μm) (S2), cycled at 0.1 C (0.1 C: 20 mA/g) and 25 °C.

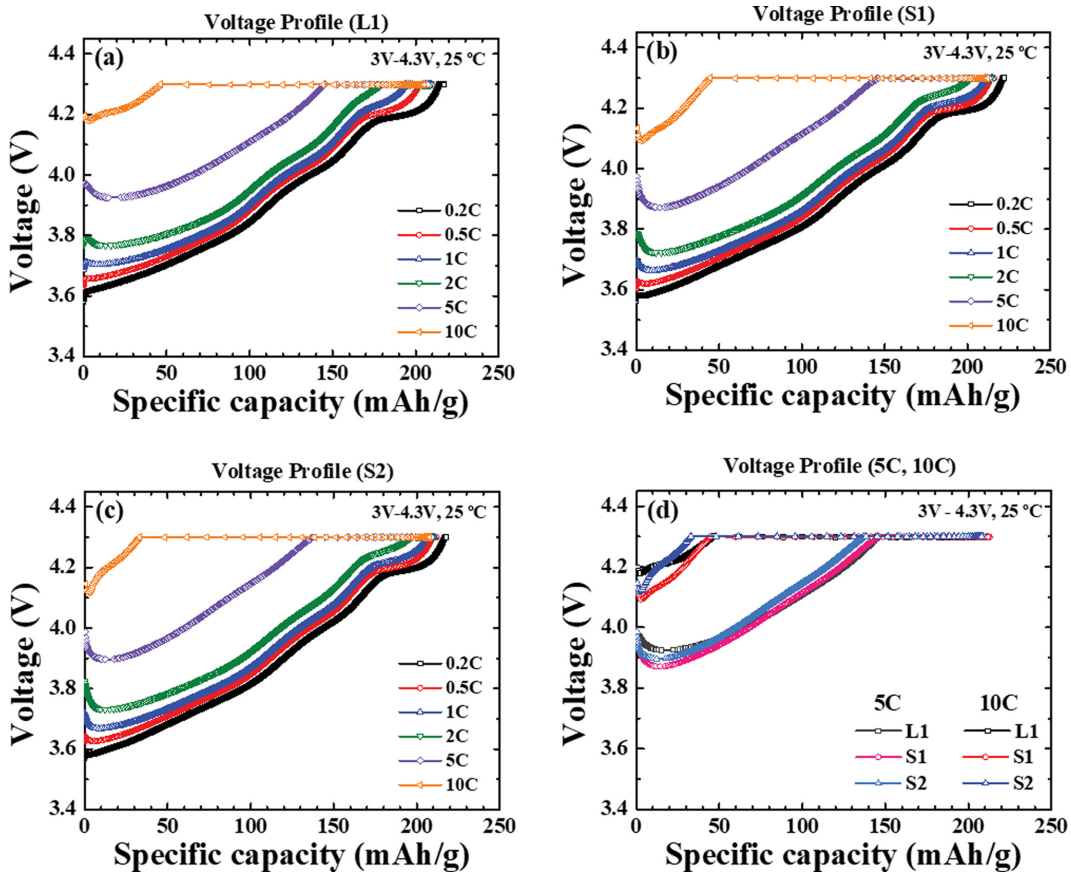

Fig. 3. Charge voltage profiles of (a) secondary particle (L1), (b) single particle (<1 μm) (S1), (c) single particle (>1 μm) (S2) at 0.2 C, 0.5 C, 1 C, 2 C, 5 C, and 10 C with increasing c-rate. (d) Comparison of fast-charging performance as the charge curves of cathode particles with different morphology (L1, S1, S2) at 5 C, 10 C rate.

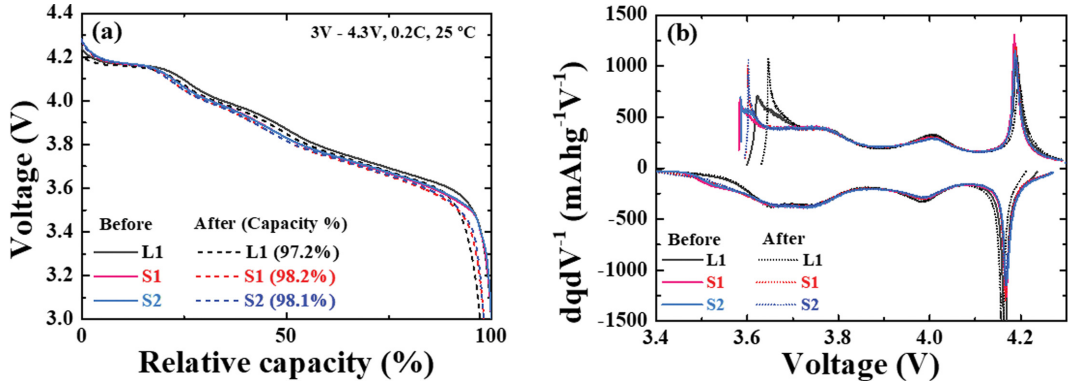

Fig. 4. (a) Comparison of relative capacity (%) at cycles before and after fast-charging for secondary particle (L1), single particle (<1 μm) (S1), single particle (>1 μm) (S2). (b) Differential capacity profiles obtained by differentiating the charge–discharge voltage profiles at cycles before and after fast-charging for L1, S1, S2.

rials, S1 having a smaller crystal size (<1 μm) exhibits a larger initial capacity than that of S2.

3. Fast-Charging Performance

To find the effect of the primary/secondary particle size on the fast-charging characteristics, an electrochemical test was performed by increasing the charge rate from 0.2 C to 10 C for the three types of high-nickel cathode materials, as shown in Fig. 3. In all particles, the overpotential increased and the proportion of the constant current (CC) in the entire charge curve was reduced with raising the current rate, as shown in Figs. 3(a)-(c). In the 5 C and 10 C charge curves (Fig. 3(d)), of single crystal S1 with the smallest particle size displays the lowest the initial overpotential and the excellent CC capacity. Secondary particle type L1 shows large initial overpotential, Nevertheless, the capacity of the cc region is similar

to that of S1 since the voltage rises slowly during fast charging. Conversely, in the case of single crystal S2 with the largest primary particles (1-2 μm), the initial overpotential is lower than L1; however, due to the large voltage slope at continuous fast charging, resulting in lower CC capacity % compared to L1 and S1. The rate capability characteristics of cathode materials are simultaneously affected by the interfacial resistance and the lithium diffusion resistance of the particles. In the case of the initial overpotential, since there is no lithium concentration gradient at the beginning of charging, it is more affected by the surface resistance and the number of lithium diffusion channels [7,8]. Therefore, the S1, which has a small particle size and a large specific surface area, shows the lowest overpotential. However, as charging continues, a concentration gradient of lithium in the cathode particle occurs and the effect of bulk diffusion through the crystal dominates [7,9,10]. In L1, since the primary particle size is the smallest, lithium can easily diffuse from the inside of the crystal to the grain boundary, consequently showing the lowest voltage slope during continuous charging. In the case of S2, the lithium diffusion distance is longer than that of other particles because the primary particles are relatively large. As a result, lithium inside the crystal cannot easily escape to the outside the crystal; thus, a large voltage increase is observed during continuous fast charging.

To examine the effect of fast charging on the cathode degradation, 0.2 C discharge capacity before and after fast charging from 0.2 C to 10 C was compared. Fig. 4(a) shows relative capacity % at cycles before and after fast-charging for each particle. The discharge capacity of all samples decreased. Among them, S1 and S2 having a single crystal morphology show better capacity retention compared with L1 with secondary particle shape. Also, S1 and S2 exhibit almost the same discharge curve after fast charging test. On the other hand, in the case of L1, a change in the voltage profile is observed, due to an increase in overvoltage after rapid charging, as shown in Fig. 4(a).

The cathode capacity loss is mainly affected by structure degradation caused by oxygen release from the particle surface, reactions with the electrolyte, and internal cracks caused by crystal volume change during charge/discharge cycling. Considering that the capacity decrease was larger in L1 with a small initial specific surface area, it can be considered that the generation of intergranular cracks along the grain boundary of secondary particles had a significant effect on the capacity loss after fast charging. In the case of single crystal type S1 and S2 with no or few grain boundaries, although the initial specific surface area is large, the subsequent increase in

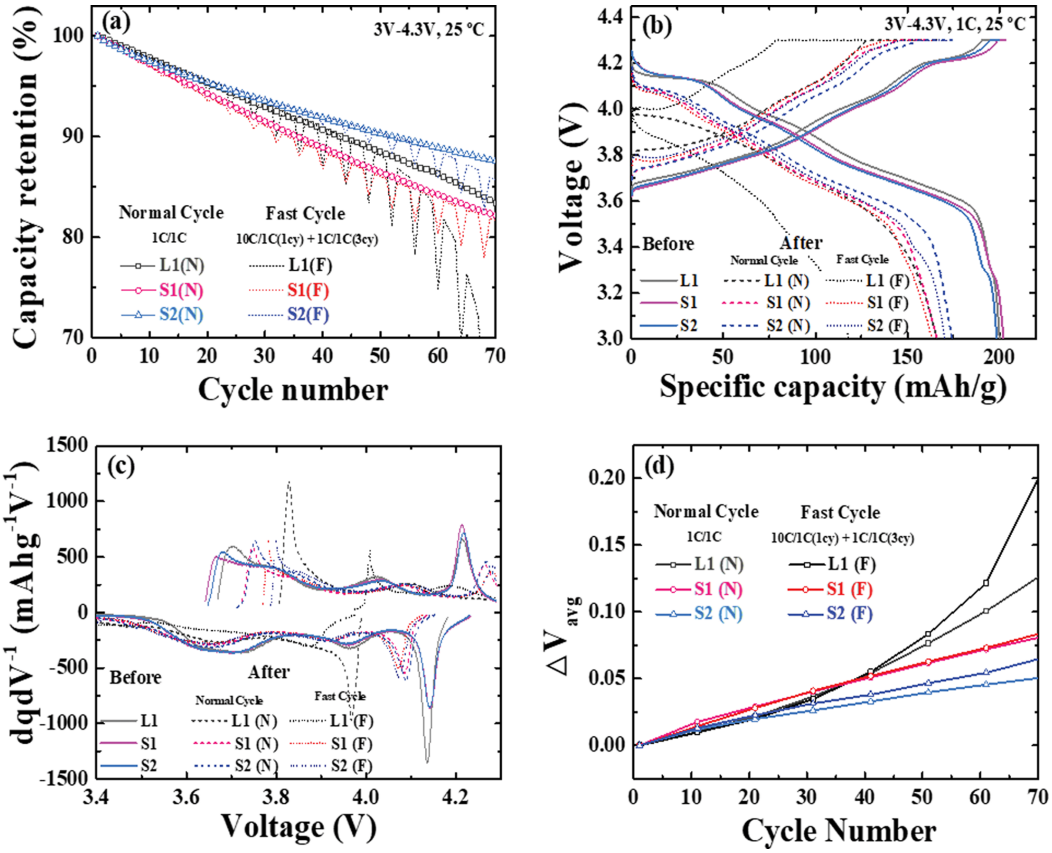

Fig. 5. (a) Cycling performance of secondary particle (L1), single particle (<1 μm) (S1), single particle (>1 μm) (S2) at 1 C (Normal Cycle), and 10 C/1 C (1cycle)+1 C/1 C (3 cycles) (Fast Cycle), and 25 °C (b) Charge-discharge curves of L1, S1, S2 at cycles before and after cycling (1st cycle and 70th cycle), cycled at 1 C and 25 °C. (c) Differential capacity profiles obtained by differentiating the charge–discharge voltage profiles at cycles before and after cycling (1st cycle and 70th cycle) for L1, S1, S2. (d) delta V (difference between the average discharge voltage) as a function of cycle number for L1, S1, S2 (Normal, Fast Cycle) measured at 25 C (between 3.0 and 4.3 V) for 70 cycles.

the specific surface area will be small and, consequently, the structural degradation after rapid charging is not accelerated.

This can also be identified from the dq/dV graph (Fig. 4(b)). In the case of S1 and S2 having a single crystal morphology, the position of the H2/H3 peak near 4.15 V, which is a characteristic peak of high-nickel layered material, hardly changed even after the fast charging, whereas the H2/H3 peak position of L1 slightly moved. It may be seen that this H2/H3 peak change is affected by the acceleration of the side reaction with the electrolyte caused by the internal crack and the consequential electrical disconnection after fast charging.

4. Cycle-Life Performance at Fast Charging

To find the effect of repeated charge/discharge on cathode degradation, capacity retention characteristics of general normal cycle and fast cycle including 10 C charge were compared for each particle. Fig. 5(a) shows cycling performance of secondary particle (L1) and single particles with different crystal size (S1, S2) at normal (1 C/1 C) and patterned fast cycle (10 C/1 C (1 cycle)+1 C/1 C (3 cycles), repeatedly). Also, to suppress the capacity in the constant-voltage region, the total charging time at 10 C was limited to 30 minutes. When comparing the fast and normal cycle, the discharge capacity remains the same at the beginning of the cycle, but as the cycle progresses, the capacity during fast cycling decreases relatively quickly compared to normal cycling due to the increased resistance caused by fast charging. Among the particles, large single crystal type S2 shows the best cycling performance in both normal and fast cycle because fewer cracks are generated inside the particles and the specific surface area is relatively smaller than that of S1, resulting in reduced side reactions at the surface. However, the difference in capacity between normal and fast cycle is relatively small in S1, which is due to the relatively small size of the primary particles and resulting excellent lithium diffusion properties [3,7]. In the case of L1 in the form of secondary particles, the initial cycle-life characteristics are relatively superior to those of S1 and S2. This could be interpreted as that a relatively small side reaction is generated at the beginning of cycle because of the small initial specific surface area of L1 (~15 μm). However, as the cycle progresses, the surface that can react with an electrolyte increases rapidly due to the generation of internal cracks in the secondary particles [6,11-14]. Therefore, side reactions occurring on the surface and the resulting capacity decrease in L1 are accelerated as the cycle progresses.

Fig. 5(b) shows the charge/discharge curves of each particle before and after normal/fast cycling (1st cycle and 70th cycle). In the case of secondary particle L1, a large overpotential occurs because of the structural degradation mentioned above. Accordingly, a sharp decrease in the capacity occurs in L1 after cycle test. On the other hand, it can be seen that the capacity loss and the resistance increase are relatively small in S1 and S2 with a single crystal morphology. In addition, as shown in the dq/dV curves of Fig. 5(c), H2/H3 peaks still exist after normal/fast cycle, although the peak positions of S1 and S2 are moved due to an increase in resistance during cycling. Moreover, even after the fast charging test, the peak position of the H2/H3 peaks is almost similar to the case of normal cycling. Whereas in the case of L1 with secondary particle type, H2/H3 peak shows large shift after normal cycle, and the peak disappears after the fast cycle test. It can be seen that the infiltration of the electrolyte caused by a crack accelerates the degradation of the secondary-particle structure [15-17].

To identify the resistance increase in high-nickel cathode material during repeated cycles, the change in the average voltage was compared every ten cycles by checking the voltage at the half of the discharge capacity (Fig. 5(d)). Similar to the capacity retention results, single crystal S2 with a large primary particle size shows the smallest change in the average voltage. In the case of S1, the resistance increase in the initial stage is larger than other particles due to its small particle size and large specific surface area. Nevertheless, there is no internal crack generation because of the single crystal morphology of S1 and, therefore, the average voltage change is suppressed as the cycle progresses. Conversely, the initial voltage change is relatively small in L1, having the morphology of secondary particles. However, the change in the average voltage continually increases as the cycle progresses and is further accelerated especially during fast cycle. This also supports the acceleration of structure degradation due to the intergranular crack in the secondary particle with the fast charging as described above.

To verify that the resistance increase gives rise to the voltage change, electrochemical impedance before and after patterned fast cycle (50 cycles) was measured for secondary particle (L1) and >1 μm sized single particle (S2). As shown in Fig. 6, L1 and S2 exhibit similar charge-transfer resistance before cycling. However, the semicircles of L1 increase more significantly after the rapid charging cycle than S2. This result is consistent with the average-voltage drop during the fast cycle (Fig. 5(d)).

Additionally, to check the degree of intergranular crack after repeated-fast charging, SEM images of electrode before and after patterned fast cycle were also measured (Fig. 7). In the case of secondary particle L1, some cracks already occur due to electrode pressing even before the fast charging. However, after rapid charging

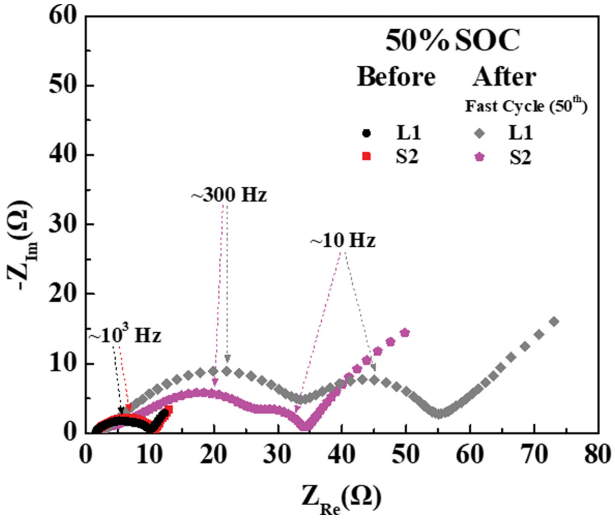

Fig. 6. Comparison of electrochemical impedance spectra of the coin cells assembled with secondary particle (L1) and single particle (>1 μm) (S2), respectively, before and after patterned fast cycle (50th) in the 1 MHz-10 mHz frequency range at 50% SOC and 25 °C.

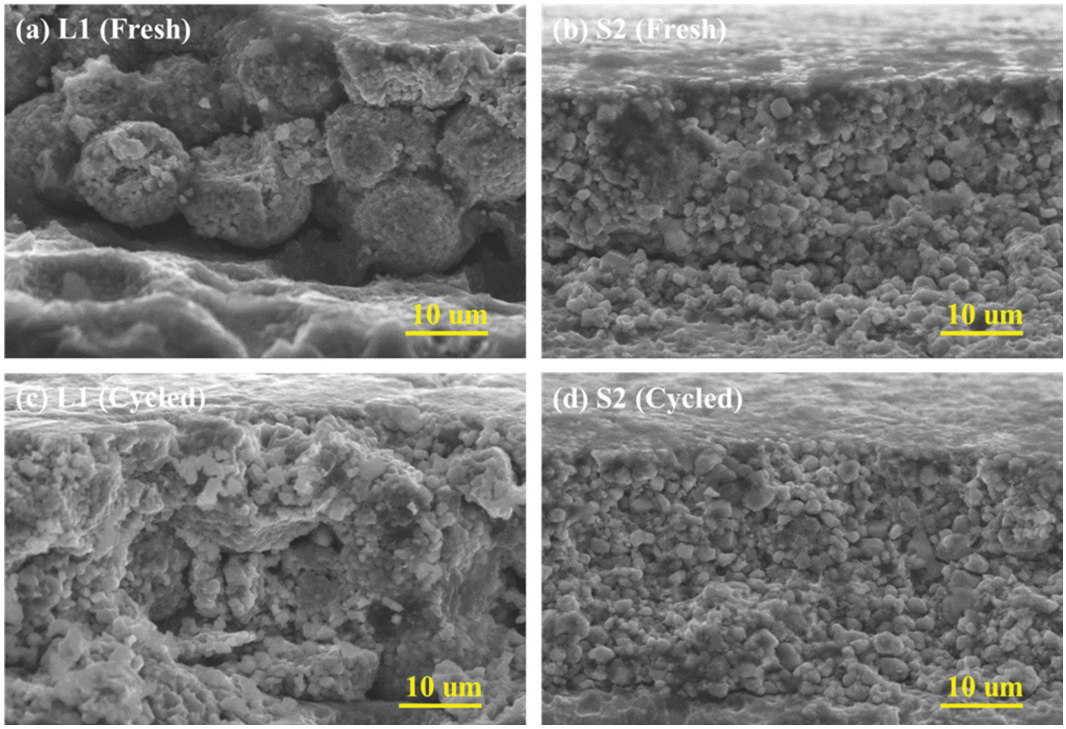

Fig. 7. SEM images of fresh electrode: (a) secondary particle (L1) and (b) >1 μm single particle (S2), and electrode after patterned fast cycle (50^{th}): (c) L1 and (d) S2.

(50 cycles), intergranular crack in the secondary particle is generated significantly and the shape of the secondary particles cannot be maintained due to the volume change that occurred during charging/discharging. On the other hand, in the case of the electrode composed of single crystal S2, the morphology of the electrode before and after rapid charging hardly changes. This shows that crack generation due to repeated fast charging is mainly induced at the grain boundary, and single crystals without grain boundaries are hardly affected by volume change during fast charging [3].

CONCLUSION

To find the effect of particle morphology on the fast charging characteristics of high-nickel materials, electrochemical tests, including various current-rate charging and repeated fast charging, were performed on the secondary particle and two single particles with different crystalline size. The particles with a relatively small crystalline size showed better initial fast charging characteristics. On the other hand, the single crystal type particle without grain boundaries exhibited better structural stability after rapid charging. In addition, repeated fast cycle further accelerates structural degradation, including intergranular cracking, which is confirmed through the SEM image, average voltage change, impedance growth, and the change of pick position in the dq/dV curve. It has been shown that the lithium diffusion, side reaction at the surface, and the deterioration due to cracks occurring inside the particles simultaneously influence the fast-charging properties of high-nickel particles. Therefore, a systematic approach including morphology control of primary/secondary particle is required to improve the fast-charging performance of high-nickel cathode materials.

ACKNOWLEDGEMENTS

This research was supported by Nano·Material Technology Development Program through the National Research Foundation of Korea(NRF) funded by Ministry of Science and ICT (NRF-2021 M3H4A6A03103719) and the Technology Innovation Program (Grant No. 20007045) funded by the Ministry of Trade, Industry & Energy (MOTIE, Korea).

REFERENCES

1. W. Li, E. M. Erickson and A. Manthiram, *Nat. Energy*, **5**, 26 (2020).
2. H.-J. Noh, S. Youn, C. S. Yoon and Y.-K. Sun, *J. Power Sources*, **233**, 121 (2013).
3. Y. Lu, T. Zhu, E. McShane, B. D. McCloskey and G. Chen, *Small*, **18**, 2105833 (2022).
4. J. Li, A. R. Cameron, H. Li, S. Glazier, D. Xiong, M. Chatzidakis, J. Allen, G. A. Botton and J. R. Dahn, *J. Electrochem. Soc.*, **164**, A1534 (2017).
5. C. Hong, Q. Leng, J. Zhua, S. Zheng, H. He, Y. Li, R. Liu, J. Wan and Y. Yang, *J. Mater. Chem. A*, **8**, 8540 (2020).
6. S. Schweidler, L. de Biasi, G. Garcia, A. Mazilkin, P. Hartmann, T. Brezesinski and J. Janek, *ACS Appl. Energy Mater.*, **2**, 7375 (2019).
7. E. Trevisanello, R. Ruess, G. Conforto, F. H. Richter and J. Janek, *Adv. Energy Mater.*, **11**, 2003400 (2021).
8. T. Aida, T. Toma and S. Kanada, *J. Solid State Electrochem.*, **24**, 1415 (2020).

9. M. Ge, S. Wi, X. Liu, J. Bai, S. Ehrlich, D. Lu, W.-K. Lee, Z. Chen and F. Wang, *Angew. Chem. Int. Ed.*, **60**, 17350 (2021).
10. X. He, H. Sun, X. Ding and K. Zhao, *J. Phys. Chem. C*, **125**, 10284 (2021).
11. L. de Biasi, B. Schwarz, T. Brezesinski, P. Hartmann, J. Janek and H. Ehrenberg, *Adv. Mater.*, **31**, 1900985 (2019).
12. W. Wei, Z. Ding, C. Chen, C. Yang, B. Han, L. Xiao, C. Liang, P. Gao and K. Cho, *Acta Materialia*, **212**, 116914 (2021).
13. T. Li, X.-Z. Yuan, L. Zhang, D. Song, K. Shi and C. Bock, *Electrochem. Energy Rev.*, **3**, 43 (2020).
14. S. Yin, W. Deng, J. Chen, X. Gao, G. Zou, H. Hou and X. Ji, *Nano Energy*, **83**, 105854 (2021).
15. C.-H. Jung, D.-H. Kim, D. Eum, K.-H Kim, J. H. Choi, J. W. Lee, H.-H. Kim, K. S. Kang and S.-H. Hong, *Adv. Funct. Mater.*, **31**, 2010095 (2021).
16. H.-H. Ryu, B. Namkoong, J.-H. Kim, I. Belharouak, C. S. Yoon and Y.-K. Sun, *ACS Energy Lett.*, **6**, 2726 (2021).
17. C. Xu, P. J. Reeves, Q. Jacquet and C. P. Grey, *Adv. Energy Mater.*, **11**, 2003404 (2021).